

Calibrating the Radio Neutrino Observatory in Greenland

Philipp Windischhofer^{a,*} on behalf of the RNO-G collaboration

^a*University of Chicago,
5640 S. Ellis Ave, Chicago, USA*

E-mail: windischhofer@uchicago.edu

The Radio Neutrino Observatory in Greenland (RNO-G) targets the detection of ultra-high energy neutrinos by observing radio emissions from neutrino-induced particle showers in glacial ice. At completion, RNO-G will consist of 35 autonomous antenna stations distributed over $O(50 \text{ km}^2)$. The physics program of this unique instrument requires excellent understanding of the detector response, the geometry of the deployed antenna stations, and the electrical properties of the surrounding glacial ice. This document provides an overview of the calibration techniques developed to address these challenges and shows their application to the seven already-operational RNO-G stations.

*10th International Workshop on Acoustic and Radio EeV Neutrino Detection Activities (ARENA2024)
11-14 June 2024
The Kavli Institute for Cosmological Physics, Chicago, IL, USA*

*Speaker

1. Introduction

The Radio Neutrino Observatory in Greenland (RNO-G) is an autonomous-station radio array currently under deployment near Summit Station, Greenland, targeting the detection of neutrinos in the EeV energy range [1]. Each RNO-G station follows a triangular layout and is equipped with 24 antenna channels, including both a deep in-borehole (at up to 100 m depth) as well as a surface component (cf. Figure 3a and Ref. [1]). At the time of writing, the array comprises seven stations in science operation, with the deployment of a total of 35 stations firmly planned.

The RNO-G physics program requires calibration of the detector in two related, but non-equivalent ways. First, the calibration of recorded *data* in order to remove nonidealities introduced by the data acquisition system; and second, the calibration of the detector *simulation model* to ensure that it faithfully represents the deployed instrument on a per-channel basis. Taken together, this allows data from different detector stations (deployed with potentially different hardware revisions) to be efficiently analyzed together, and ensures that the energy scale and direction information of (neutrino) candidate events can be accurately reconstructed [2, 3].

This proceedings article gives an overview of the aspects of the RNO-G design requiring calibration and summarizes the calibration strategies developed on the way to first physics. The component-level calibration of the analog signal path is described in Section 2, while Section 3 covers the calibration of the station antenna geometry and the properties of the surrounding glacial ice. The RNO-G calibration efforts have also previously been reported on in Ref. [4].

2. Signal Path Modeling and Calibration

The RNO-G science antennas are connected to the data acquisition system through a multi-component analog signal path, which transports, amplifies, and conditions the weak radio-frequency (RF) signal ahead of digitization, targeting the 80–650 MHz band [5]. Figure 1 illustrates the signal path for a down-hole channel, consisting of a low-noise amplifier situated close to the antenna, an RF-over-fiber link to the surface, and a secondary amplification stage followed by the digitizer.

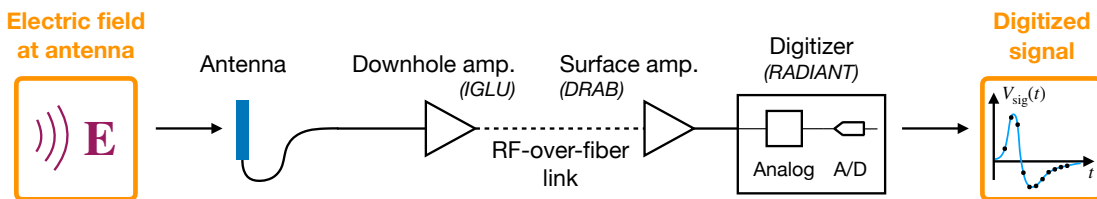


Figure 1: Schematic overview of the signal path for an RNO-G down-hole channel as relevant for calibration purposes, consisting of a low-noise down-hole amplifier (*IGLU*) which is connected to a surface amplifier (*DRAB*) through an RF-over-fiber link. Also shown is the digitizer board (*RADIANT*).

2.1 Signal Path Characterization

Before deployment, a specific combination of amplifiers and fibers is assigned to each antenna channel and the full analog signal chain is assembled in the laboratory. Measurements of the end-to-end scattering matrix are taken across the passband and recorded in a calibration database,

from where they are retrieved on-demand and used to model the channel response in the simulation framework NuRadioMC [6]. Of particular importance is the modeling of the total forward gain and the total group delay, which are connected to the inferred (neutrino) energy scale and event localization, respectively.

Scattering parameters of all active components and fibers are also measured separately, allowing the simulated channel response to be kept up-to-date in the event a replacement of individual components during (or following) deployment becomes necessary.

2.2 Digitizer Calibration

The RNO-G data acquisition system utilizes the *LAB4D* switched-capacitor array 12-bit analog-to-digital converter [7] for each channel, housed on the *RADIANT* digitizer board [1]. The transfer curve of each LAB4D unit can be measured in-situ in a fully-automated fashion to enforce the linearity of the voltage scale for each channel and to monitor the temperature-dependence and general stability of the deployed digitizer system.

For this purpose, the *RADIANT* board is equipped with a high-accuracy digital-to-analog converter that injects a slow-ramping quasi-DC voltage into the LAB4D inputs. At present, digitizer calibration data is taken approximately once per day; Figure 2a shows an example LAB4D transfer curve obtained with this system.

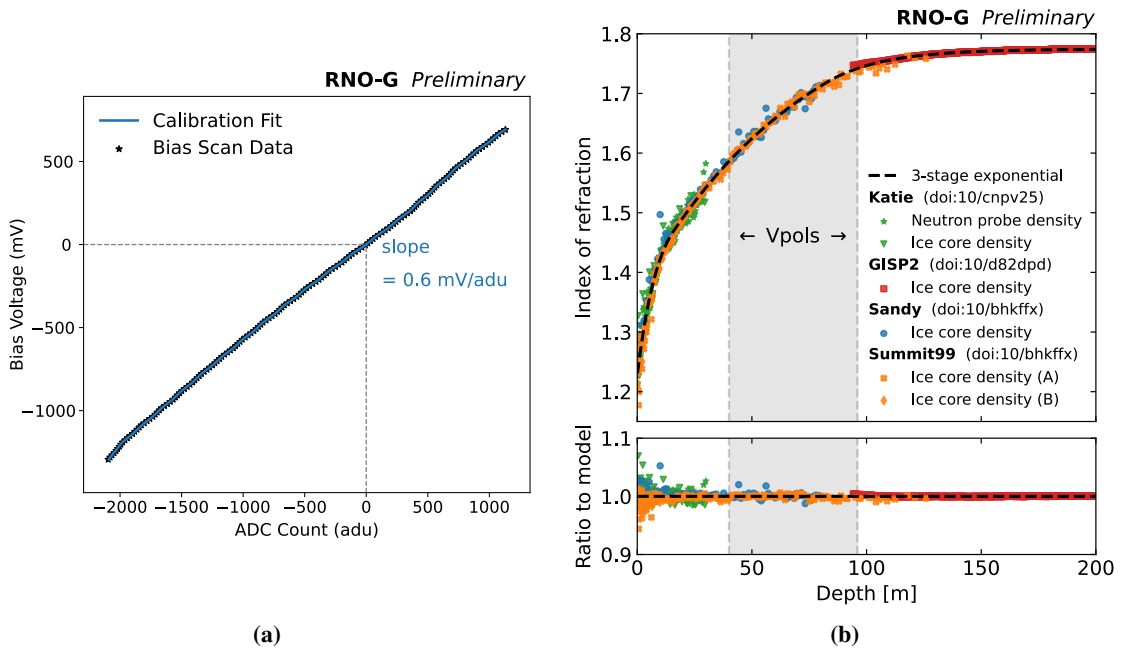


Figure 2: (a) Example transfer curve of the LAB4D digitizer as measured by the on-board calibration system. (b) Refractive index profile of the glacial ice near Summit Station, as obtained from ice core density measurements (references given in the Figure). The dashed black curve is a fit of a three-stage exponential function, and the vertical gray area indicates the approximate depth of the RNO-G down-hole antennas.

3. Station Geometry Calibration and Ice Modeling

To be able to reconstruct (neutrino) candidate events from the recorded time-domain antenna signals, the positions of the science antennas in a deployed RNO-G station and the depth profile of the refractive index of the ice surrounding the station must be accurately known.

This poses significant challenges for the down-hole antennas, whose locations cannot directly be surveyed with GPS, but for which only measurements of the borehole location on the surface are available. Similarly, the refractive-index depth profile is accessible indirectly through ice core density measurements (cf. Section 3.1), and the electrodynamic properties of the bulk ice can be captured by radioglaciological methods [4, 8, 9].

To reduce uncertainties, these “prior” measurements of antenna positions and refractive index profile are subsequently updated through timing-based corrections (cf. Sections 3.2 and 3.3).

3.1 Ice Refractive Index

Figure 2b shows the dependence of the depth profile $n(z)$ of the refractive index of the glacial ice near Summit Station, as inferred from measurements of the local density profile $\rho(z)$ near Summit Station through the relation

$$n(z) = 1 + c_0 \cdot \rho(z), \quad (1)$$

where $c_0 = 0.845 \text{ cm}^3 \text{ g}^{-1}$ [10]. Below a depth of around 20 m, the refractive index is well-described by a three-stage piecewise-exponential profile, as expected from a three-phase glaciological densification model [11].

3.2 In-Situ Position Calibration

Each RNO-G station is equipped with three calibration pulsers (cf. Figure 3a) at well-defined locations relative to the science antennas. The calibration pulsers emit impulsive signals (cf. Figure 3b), whose arrival time differences between pairs of science antennas provide sensitivity to the station geometry and the refractive index profile.

To extract these constraints, a maximum-likelihood fit is performed to the calibration pulser timing dataset, into which the positions of the three RNO-G antenna strings and the antenna depths along each string are introduced as free parameters. The refractive index profile is modeled as a three-stage piecewise-exponential function as obtained from the ice core density measurements explained in Section 3.1. The shape of the $n(z)$ -profile is kept fixed in the fit, but a depth-independent multiplicative scale factor is introduced as additional free parameter to adjust the value of the dimensionful constant c_0 relative to its literature value in Eq. 1.

Figure 4 shows the resulting best-fit antenna positions for RNO-G station 11. The corrections to the string positions are of the order of 0.5 m, with the relative vertical spacing of the antennas on the same string remaining very stable throughout. Uncertainties on the postfit string positions are in the range 0.3–0.4 m. The constant c_0 in Eq. 1 is adjusted by around 1%, with a postfit uncertainty in a similar range.

3.3 Additional Position Calibration Sources

Some deformations of the station geometry cannot be constrained by the in-situ position calibration alone. In particular, the absolute position of the station and its orientation relative to the ice

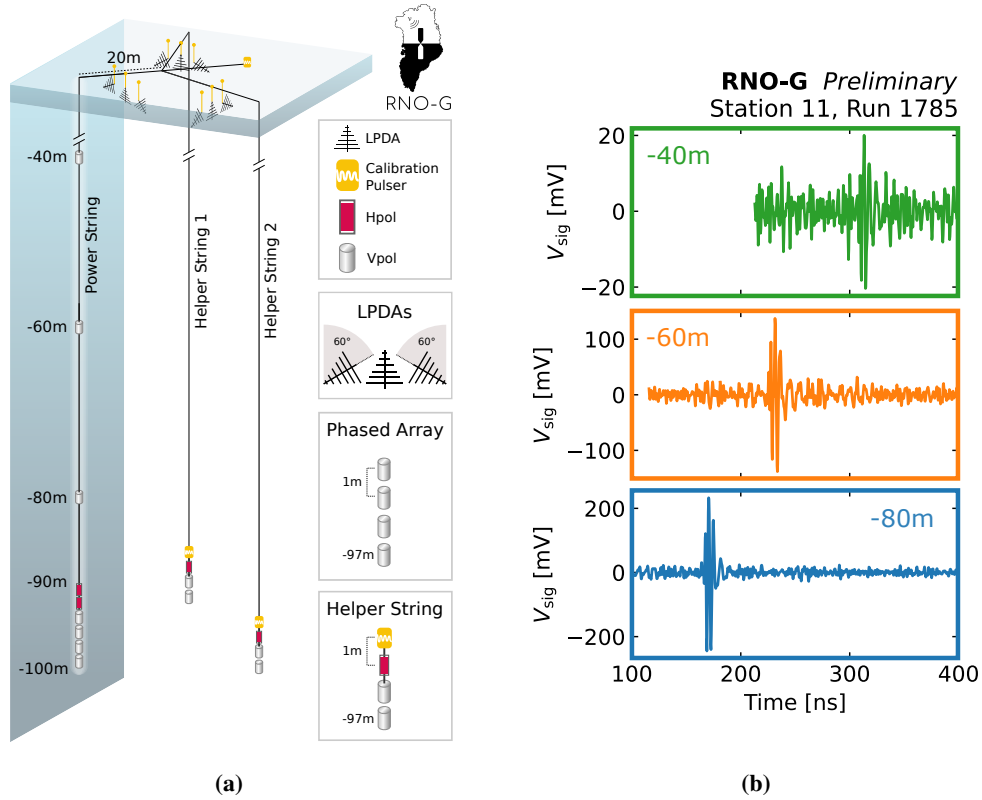


Figure 3: (a) Schematic view of an RNO-G station with the three in-situ calibration pulsers shown in yellow. (b) Signals observed in the topmost three antennas (at depths of 40 m, 60 m, and 80 m) on the Power String in response to a pulse emitted by the calibration pulser on Helper String 2.

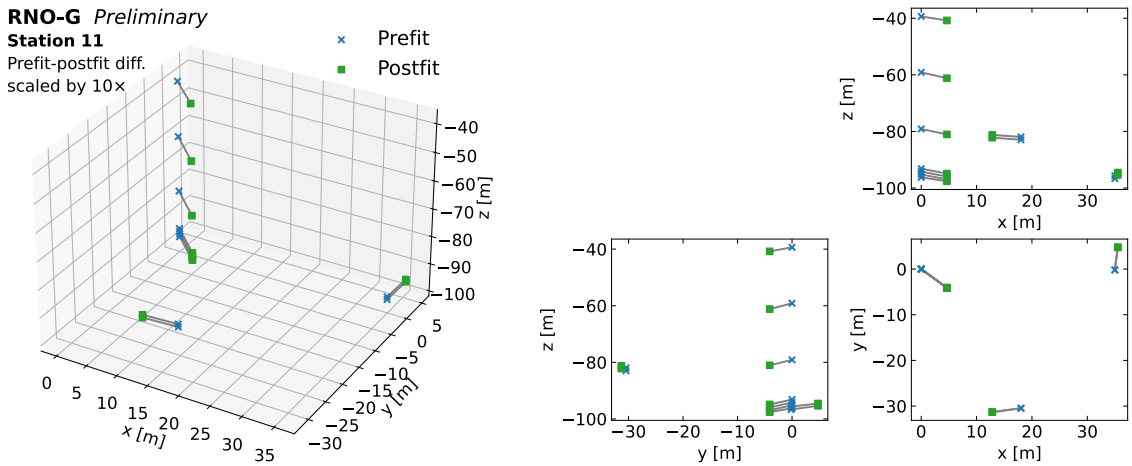


Figure 4: Positions of the down-hole antennas in RNO-G station 11 based on GPS survey and depth measurements (“prefit”), and after corrections from the in-situ calibration have been applied (“postfit”). The prefit–postfit difference is scaled by 10× for visualization purposes.

surface remain unconstrained. Additional calibration data is available from station-external radio sources that can impose independent constraints on the station geometry and/or reduce the impact of systematic uncertainties on the calibration. Two complementary calibration sources are briefly described below. Work is presently ongoing to include these data into a global position calibration fit.

3.3.1 Opportunistic Radio Sources: Air Planes and Solar Flares

Impulsive signals from solar flares [12] or airplane radar altimeters [13] have been reliably identified in RNO-G data. Both signals originate from point radio sources whose positions are independently known, and thus form potentially very valuable calibration sources. Work is currently underway to integrate these data into the array-wide calibration fit.

3.3.2 Diffuse Radio Sources: Thermal Noise

The RNO-G detector is embedded in the diffuse field of thermal electromagnetic radiation emitted by the surrounding ice. Contrary to noise generated by amplifiers and resistive elements in the readout chain, this environmental thermal noise is *correlated* between different channels, with the degree of correlation depending on the spatial separation of the corresponding antennas.

It is a surprising consequence of fluctuational electrodynamics [14] that this correlation pattern can be used to measure the absolute signal travel time as well as the relative cable delay for any pair of receiving antennas. This extraction happens in an entirely passive way, i.e. no pulsing antenna is necessary.

Specifically, the quantity of interest is the per-event cross-correlation of the noise voltage signals $V_A(t)$ and $V_B(t)$ that appears at the feeds of antennas A and B , averaged over the available dataset,

$$\langle C_{AB}(\Delta t) \rangle := \langle V_A(t) \star V_B(t) \rangle = \frac{1}{N} \sum_{i=1}^N V_{A,i}(t) \star V_{B,i}(t), \quad (2)$$

where \star denotes cross-correlation and the dataset is taken to consist of N noise events. The averaged cross-correlator $\langle C_{AB}(\Delta t) \rangle$ can be shown to depend on the impulse response $G_{AB}(t)$, i.e. the voltage signal that is observable at the feed of antenna B if a Dirac-delta like current is injected into antenna A ,

$$\langle C_{AB}(\Delta t) \rangle \sim k_B T \mathcal{F}^{-1} [\text{Re } G_{AB}(\omega)]. \quad (3)$$

In this relation, \mathcal{F}^{-1} denotes the inverse Fourier transform, k_B is the Boltzmann constant, and T is the absolute temperature of the ice. In particular, this shows that $\langle C_{AB} \rangle$ is symmetric, $C_{AB}(\Delta t) = C_{AB}(-\Delta t)$, and if the absolute signal travel time between antennas A and B is t_{AB} , Eq. 3 predicts that significant correlation exists for $\Delta t_{1,2} = \pm t_{AB}$. If fiber group delays t_A^F and t_B^F are included, maximum-correlation is instead attained at $\Delta t_{1,2} = (\pm t_{AB}) + (t_A^F - t_B^F)$.

Conversely, calculating the averaged correlator according to Eq. 2 based on the available noise dataset and identifying $\Delta t_{1,2}$ allows the absolute propagation time t_{AB} and the relative cable delay $t_A^F - t_B^F$ to be identified in-situ. Figure 5 shows an example of this technique applied to RNO-G station 11, yielding propagation times and relative cable delays consistent with expectations.

As the deployed RNO-G stations continue to integrate (noise) data, this technique has the potential to become an increasingly powerful complement to the in-situ calibration pulser dataset.

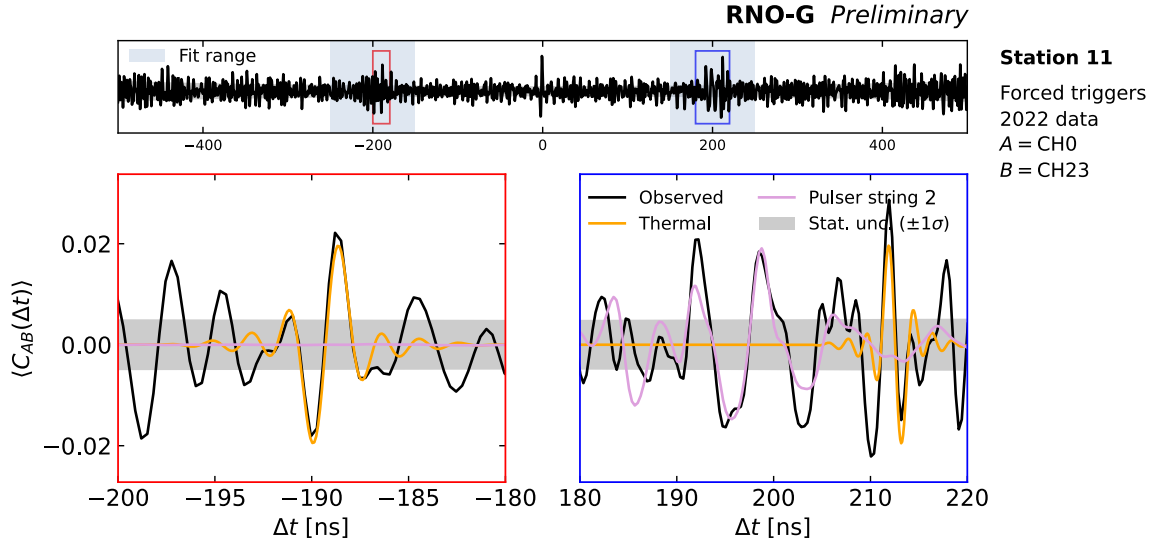


Figure 5: Averaged cross-correlation of thermal noise data (black) between the bottommost antennas on the Power String (CH0) and Helper String 2 (CH23) on RNO-G station 11. The prediction for $\langle C_{AB} \rangle$ according to Eq. 3 is shown in orange, and the purple line is the contribution from the calibration pulser on Helper String 2, which, although not actively pulsing, acts as a point-like noise source. The normalization of the respective components have been determined through a fit to the observed correlator. The averaging is performed over $N \approx 500 \cdot 10^3$ events.

4. Conclusions and Outlook

A diverse suite of calibration techniques has been developed to build the detailed understanding of the RNO-G instrument that is required to fully exploit its science potential. This includes protocols for the laboratory characterization of all detector channels as well as methods to determine the geometry of each deployed antenna station and study the properties of the surrounding glacial ice.

These strategies, and the technical and simulation infrastructure supporting them, have been designed to scale to the full 35-station array, preparing the ground for efficient array-wide data analysis as detector deployment is set to continue during the upcoming field campaigns.

Acknowledgments

We are thankful to the support staff at Summit Station for making RNO-G possible. We also acknowledge our colleagues from the British Antarctic Survey for building and operating the BigRAID drill for our project. We would like to acknowledge our home institutions and funding agencies for supporting the RNO-G work; in particular the Belgian Funds for Scientific Research (FRS-FNRS and FWO) and the FWO programme for International Research Infrastructure (IRI), the National Science Foundation (NSF Award IDs 2118315, 2112352, 2111232, 2112352, 2111410, and collaborative awards 2310122 through 2310129), and the IceCube EPSCoR Initiative (Award ID 2019597), the German research foundation (DFG, Grant NE 2031/2-1), the Helmholtz Association (Initiative and Networking Fund, W2/W3 Program), the Swedish Research Council (VR, Grant 2021-05449 and 2021-00158), the Carl Tryggers foundation (Grant CTS 21:1367), the University

of Chicago Research Computing Center, and the European Union under the European Unions Horizon 2020 research and innovation programme (grant agreements No 805486), as well as (ERC, Pro-RNO-G No 101115122 and NuRadioOpt No 101116890).

References

- [1] J.A. Aguilar et al., “Design and sensitivity of the Radio Neutrino Observatory in Greenland (RNO-G)”, *JINST* 16, P03025 (2021)
- [2] I. Plaisier, S. Bouma, A. Nelles, “Reconstructing the arrival direction of neutrinos in deep in-ice radio detectors”, *Eur. Phys. J. C* 83, 443 (2023)
- [3] J.A. Aguilar, P. Allison, J.J. Beatty et al., “Reconstructing the neutrino energy for in-ice radio detectors: A study for the Radio Neutrino Observatory Greenland (RNO-G)”, *Eur. Phys. J. C* 82, 147 (2022)
- [4] C. Welling and the RNO-G Collaboration, “Calibration of the Radio Neutrino Observatory in Greenland (RNO-G)”, *PoS(ICRC 2023)*, 1054 (2023)
- [5] E. Oberla and the RNO-G Collaboration, “Low-Power Radiofrequency Systems for the RNO-G Project”, *PoS(ICRC 2023)*, 1171 (2023)
- [6] C. Glaser, D. García-Fernández, A. Nelles et al. “NuRadioMC: simulating the radio emission of neutrinos from interaction to detector”, *Eur. Phys. J. C* 80, 77 (2020)
- [7] J.M. Roberts, G.S. Varner, P.Allison et al., “LAB4D: A low power, multi-GSa/s, transient digitizer with sampling timebase trimming capabilities”, *Nucl. Instrum. Meth. A* 925, 92–100 (2019)
- [8] The RNO-G Collaboration, “Precision measurement of the index of refraction of deep glacial ice at radio frequencies at Summit Station, Greenland”, [arXiv:2304.06181 \[astro-ph.IM\]](https://arxiv.org/abs/2304.06181) (2023)
- [9] The RNO-G Collaboration, “Radiofrequency ice dielectric measurements at Summit Station, Greenland”, *Journal of Glaciology*, 1-12 (2023)
- [10] A. Kovacs, A.J. Gow, and R.M. Morey, “The in-situ dielectric constant of polar firn revisited”, *Cold Regions Science and Technology* 23, 3 (1995)
- [11] K. Couberly and the ARA Collaboration, “Modeling the refractive index profile $n(z)$ of polar ice for ultra-high energy neutrino experiments”, [arXiv:2406.00857 \[astro-ph\]](https://arxiv.org/abs/2406.00857) (2024)
- [12] The RNO-G Collaboration, “Solar flare observations with the Radio Neutrino Observatory Greenland (RNO-G)”, [arXiv:2404.14995 \[astro-ph.SR\]](https://arxiv.org/abs/2404.14995) (2024)
- [13] J. Stoffels and the RNO-G Collaboration, “Observation of Galactic noise and identification of background sources in RNO-G”, *PoS(ARENA 2024)*
- [14] S.M. Rytov, Yu.A. Kravtsov, V.I. Tatarskii, “Elements of statistical radiophysics”, Vol. 3, 2nd edition, pp. 109–150 (1978)